

Cite this: *J. Mater. Chem. A*, 2024, **12**, 1694

Enhancing ionic conductivity and suppressing Li dendrite formation in lithium batteries using a vinylene-linked covalent organic framework solid polymer electrolyte†

Jin Yang,^{†a} Chenxiao Lin,^{†be} Yonglei Wang,^b Yaolin Xu,^b Duong Tung Pham,^b Xiangqi Meng,^b Khanh Van Tran,^b Sijia Cao,^{bd} Nikolay Kardjilov,^b André Hilger,^b Jan Dirk Epping,^a Ingo Manke,^b Arne Thomas^{*,a} and Yan Lu^{*,bcd}

The growing demand for energy-dense and safe batteries drives research towards all-solid-state lithium (Li) batteries. Existing poly(ethylene oxide) (PEO)-based solid polymer electrolytes (SPEs) suffer from low Li⁺ conductivity and Li dendrite penetration. Covalent organic frameworks (COFs) as highly crystalline, porous, and chemically diverse organic materials show great potential to address these problems. However, extensively studied imine-linked COFs show insufficient electrochemical stability against reactive Li metal, limiting their application for Li batteries. Herein, we develop a chemically stable vinylene-linked covalent organic framework (VCOF)-based SPE. By incorporating <4 wt% VCOF-1, a 25% improvement in ionic conductivity and a 46% increase in Li⁺ transference number at 60 °C are achieved. DFT calculations reveal that VCOF-1 facilitates Li⁺ transport through its cylindrical pores aided by PEO. *In situ* X-ray tomography confirms that VCOF-1 substantially suppresses Li dendrite growth in the VCOF-SPE-based Li metal batteries attributed to the enhanced Li-ion conduction and 12-fold improved mechanical strength. VCOF-SPEs also exhibit a high capacity of ~145 mA h g⁻¹ at 0.1C in LiFePO₄/Li coin cells. Notably, the LiFePO₄/Li pouch cell withstands abuse test conditions such as folding, cutting, and nail penetration. These results demonstrate the potential of VCOFs in future all-solid-state Li metal batteries for energy storage.

Received 12th August 2023
Accepted 4th December 2023

DOI: 10.1039/d3ta04822e

rsc.li/materials-a

1 Introduction

Lithium (Li) metal batteries are particularly useful devices for sustainable energy storage due to their high energy density.^{1–3} Nevertheless, numerous challenges remain regarding their widespread use, *e.g.*, the safety risks related to hazardous Li dendrite growth and the high flammability of conventional organic liquid electrolytes.⁴ The increasing demand for safe Li metal batteries

has been driving the research toward solid-state electrolytes.^{2,3,5–9} Polyethylene oxide (PEO) based solid polymer electrolytes (SPEs) are considered promising electrolytes for all-solid-state Li metal batteries due to their electrochemical stability against Li metal and mechanical flexibility.^{2,3,10–12} However, Li dendrite growth and penetration through the PEO-based SPEs is a critical issue due to their limited mechanical strength, which causes battery failure and safety threats.^{13,14} Besides, the high crystallinity of PEO results in poor ionic conductivity (10⁻⁸ to 10⁻⁷ S cm⁻¹) at room temperature and an inferior Li-ion transference number, far from meeting the practical application requirements.¹⁵ An efficient approach to deal with the issues of PEO-based SPEs mentioned above is to add plasticizers or polymers into PEO membranes.¹⁶ The Ooyama's group found that the ionic conductivity of PEO/LiClO₄ blended with polyethylenimine (PEI) is much higher (~10⁻⁴ S cm⁻¹ at room temperature) than that of PEO/LiClO₄ electrolyte.¹⁷ The introduction of PEI could efficiently suppress the crystallization of PEO and thus sharply increase the Li-ion mobility and ionic conductivity.¹⁸

Recently, covalent organic frameworks (COFs) as crystalline and highly porous organic materials have demonstrated

^aDepartment of Chemistry/Functional Materials, Technische Universität Berlin, Hardenbergstraße 40, 10623 Berlin, Germany. E-mail: arne.thomas@tu-berlin.de

^bInstitute of Electrochemical Energy Storage, Helmholtz-Zentrum Berlin für Materialien und Energie, Hahn-Meitner-Platz 1, 14109 Berlin, Germany. E-mail: yan.lu@helmholtz-berlin.de

^cInstitute for Technical and Environmental Chemistry, Friedrich-Schiller-Universität Jena, Philosophenweg 7b, 07743 Jena, Germany

^dHelmholtz Institute for Polymers in Energy Applications (HIPOLE), Philosophenweg 7b, 07743 Jena, Germany

^eCollege of New Energy, Ningbo University of Technology, 315336 Ningbo, China

† Electronic supplementary information (ESI) available. See DOI: <https://doi.org/10.1039/d3ta04822e>

* Jin Yang and Chenxiao Lin contributed equally to this work.





Fig. 1 Synthesis and characterization of the SPEs. (a) The preparation procedure of the SPEs. (b) Crystal structure of VCOF-1 (c and a direction view). (c) Comparison of the experimental and simulated AA stacking PXRD patterns of VCOF-1 (inset: photograph of VCOF-1). (d) Photograph and (e) cross-sectional SEM images of the prepared VCOF-SPE. (f) High-resolution Li 1s XPS spectra, (g) static ^7Li ss-NMR spectra of the VCOF-SPE and Ref-SPE compared with LiTFSI. Ref-SPE represents reference SPE with the same composition as VCOF-SPE but without adding VCOF-1.

resolution XPS (Fig. 1f and S5[†]). The binding energy (BE) of Li in VCOF-SPE is located at 55.2 eV, which is different from the BE of Li in LiTFSI (56.3 eV) and Ref-SPE (54.8 eV).^{41,42} This indicates that Li ions merge and actively interact with VCOF-1 in VCOF-SPE. Finally, the ^7Li ss-NMR in Fig. 1g unambiguously proves the distinct Li chemical environment in VCOF-SPE compared to in Ref-SPE and LiTFSI.^{43,44} The ^7Li signals of VCOF-SPE and Ref-SPE become narrower and shift to a lower field compared to those of LiTFSI, indicating that PEO acts as a vital component to promote the movement of Li^+ . In addition, the higher mobility of Li^+ in VCOF-SPE than in Ref-SPE can be inferred from the ^7Li spin-lattice relaxation time (T_1), as shorter T_1 times positively correlate with better Li^+ conductivity in these composites (Fig. S6[†]). The fitted ^7Li T_1 times are reduced from 0.357 s in Ref-SPE to 0.280 s in VCOF-SPE (21.5% faster), corroborating the superior Li^+

conductivity of VCOF-SPE in comparison to that of Ref-SPE. Thermogravimetric analysis (TGA) showed a first weight loss for VCOF-SPE at $\sim 355^\circ\text{C}$, indicating the excellent thermal stability of VCOF-SPE (Fig. S7[†]). The thermal behavior of VCOF-SPE was also investigated using differential scanning calorimetry (DSC). Fig. S8[†] shows a glass transition temperature (T_g) of around -37.9°C . The second event, T_{m1} appeared at about 47.5°C and can be assigned to the gradual melting of the intermediate crystalline compound. The melting (T_{m2}) of crystalline PVDF at approximately 135°C is observed.

2.2 Electrochemical characterization and theoretical simulations of VCOF-SPE

As the key feature of the electrochemical properties of SPEs, the ionic conductivities (σ , S cm^{-1}) of VCOF-SPE and Ref-SPE were



determined by electrochemical impedance spectroscopy (EIS). Here, stainless steel|SPEs|stainless steel (SS|SPEs|SS) symmetric coin cells were assembled to obtain impedance spectra (Fig. S9†). Fig. 2a shows the temperature dependence of ionic conductivities of VCOF-SPE and Ref-SPE in the temperature range of 10–80 °C. A sharp conductivity increase was observed from 10 to 80 °C for both the VCOF-SPE and Ref-SPE. The measured conductivities of VCOF-SPE at 10 °C and 25 °C are $1.53 \times 10^{-7} \text{ S cm}^{-1}$ and $2.11 \times 10^{-6} \text{ S cm}^{-1}$, respectively, which then increases to $2.66 \times 10^{-4} \text{ S cm}^{-1}$ at 60 °C and $7.79 \times 10^{-4} \text{ S cm}^{-1}$ at 80 °C, respectively. These values are higher than those of Ref-SPE ($9.27 \times 10^{-8} \text{ S cm}^{-1}$ at 10 °C, $2.12 \times 10^{-4} \text{ S cm}^{-1}$ at 60 °C, and $6.14 \times 10^{-4} \text{ S cm}^{-1}$ at 80 °C). The ionic conductivity is increased by 25% at 60 °C by adding only 3.85 wt% of VCOF-1 into the SPE membrane. The conductivity of VCOF-SPE showed an increase with the increasing content of VCOF-1 (Fig. S10†), reaching an optimum at 3.85 wt%. Beyond this content, the conductivity started to gradually decrease. This decrease can be attributed to the combined effect of increasing Li⁺-free VCOF-1 and decreased Li⁺-containing LiTFSI, which tends to reduce conductivity. The ionic conductivities were simulated based on different SPE models. Aligning with the experimental results, a similar trend of the simulated ionic conductivity was observed for VCOF-SPEs and Ref-SPEs as the temperature changed (Fig. S11†). Also, in the atomistic simulation, VCOF-SPE exhibits a higher ionic conductivity than Ref-SPEs, which can be attributed to the stronger specific binding of TFSI anions to the VCOF-1 fragments (Fig. S12†). The nanopores in VCOFs facilitate Li-ion transport since the highly porous structure of VCOF-1 allows for the occurrence of Li-ion hopping

or/and the vehicle mechanisms.⁴⁵ Besides, the ordered, cylindrical micro- or mesopores of the COFs can provide pathways for Li-ion transport when VCOFs are used in SPEs.⁴⁶ Above all, the introduced VCOF-1 effectively decoupled the transport of Li cations and TFSI anions, leading to decreased anion mobility and thereafter enhanced cation diffusivity in electrolytes.

The enhanced Li⁺ conductivity of VCOF-SPE can also be attributed to the enhanced Li⁺ mobility as confirmed by XPS and ss-NMR results (Fig. 1f and g). Additionally, we found that the relationship between $\ln \sigma$ and $1000/T$ followed the Arrhenius behavior ($E_a = -bR$, where E_a is the activation energy for ion transport, b is the slope of the regressed linear $\ln \sigma - 1000/T$ plots, and R is the gas constant of $8.314 \text{ J mol}^{-1} \text{ K}^{-1}$). As shown in Fig. 2b, the fitted curves are divided into two linear parts. The curves align with the experimental data fitted by using the Arrhenius formula, demonstrating the typical features of ion conduction in the SPEs. The inflection points of the two curves correlated with the melting temperature of crystalline PEO from DSC results (Fig. S8†). The E_a of VCOF-SPE in the temperature range of 10–40 °C and 50–80 °C was calculated to be $131.0 \text{ kJ mol}^{-1}$ and 52.5 kJ mol^{-1} , respectively. Theoretically, the activation energy is defined as the energy barrier between adjacent coordinate sites for Li⁺ conduction. The change in the activation energy with the temperature can be explained by the improved motion of polymer chains and the gradual melting of the intermediate crystalline compound above 50 °C.

DFT calculations were further performed to elucidate the migration pathway of Li⁺ inside the VCOF-1 pores by comparing the migration energy barriers at rate-determining steps in two types of anisotropic pathways that are parallel and perpendicular

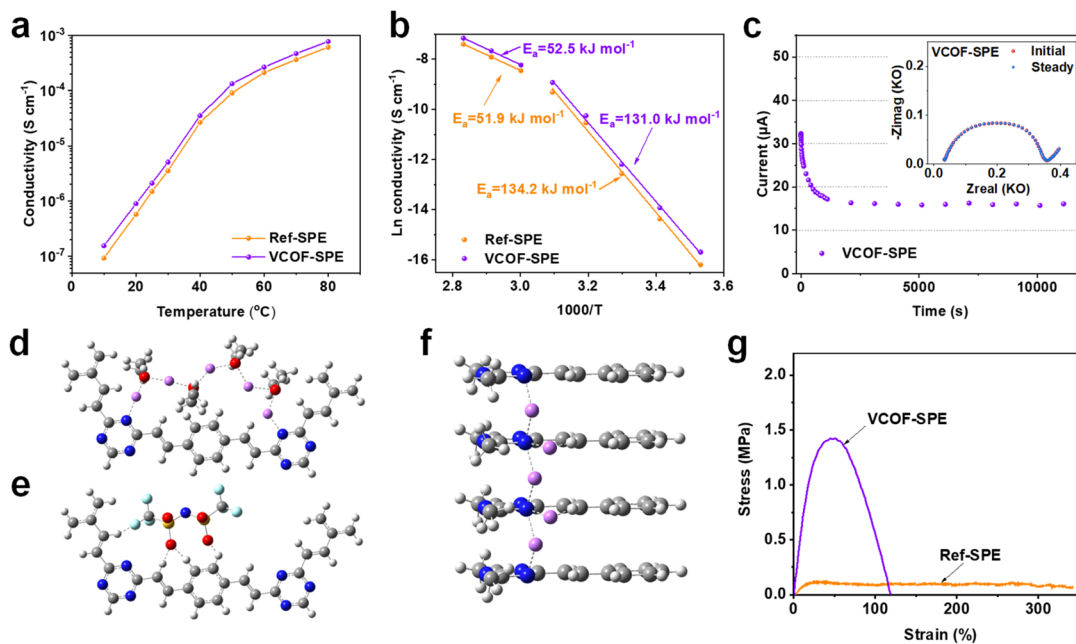


Fig. 2 (a) Temperature-dependent conductivity of VCOF-SPE and the Ref-SPE membrane. (b) Arrhenius plots of SPEs in the temperature range of 10–80 °C. (c) Chronoamperometry of the Li|VCOF-SPE|Li cell at a potential of 10 mV (inset shows the comparison of the AC impedance of the cells before and after DC polarization at 60 °C). The preferred migration pathways of Li⁺ (magenta) along with planar (d) and axial (f) directions of VCOF-1 structures and preferential interactions (e) of TFSI anions with VCOF-1 layers (C: gray; N: blue; H: white; O: red; S: yellow; F: cyan; gray stick: covalent bond; dash stick: coordinate bond). (g) Stress–strain curves of VCOF-SPE and Ref-SPE.



to axially stacked representative VCOF-1 structures (denoted as axial and planar pathways, respectively). A notable finding was that Li^+ migration in the axial pathway requires a much lower migration energy barrier ($\sim 5.7 \text{ kcal mol}^{-1}$ as shown in Fig. 2f) than the in-plane one ($\sim 26.7 \text{ kcal mol}^{-1}$ as shown in Fig. 2d). This preferred through-plane Li^+ migration pathway along the axial direction (Fig. 2f) is essentially attributed to the short hopping distances of Li^+ between neighboring VCOF-1 layers, promoted by N atoms that are adjacently aligned in the VCOF-1 crystalline structure. In addition, the H atoms in the VCOF-1 layers and O atoms in TFSI⁻ and PEO polymers can considerably enhance the thermodynamic stability of Li^+ intermediates along with the diffusion of Li^+ in the axial pathway (Fig. 2f). The hopping of Li^+ along the planar pathway (Fig. 2d) is essentially mediated by the O atoms in PEO polymers with the aid of cation–anion interactions. The Li^+ intermediates in the planar pathway are thermodynamically less favorable due to the long hopping distances between neighboring aromatic rings, and the mobility of ionic groups (PEO chains and TFSI anions) nearby further weakens the stability of Li^+ intermediates (Fig. 2e). These theoretical results demonstrate the directional Li^+ conduction along the VCOF-1 channel pores, in which the N atoms in the VCOF-1 framework play a significant role. In summary, Li^+ aided by PEO can shuttle along the cylindrical pores of VCOF-1, which promotes the Li^+ conductivity in VCOF-SPEs leading to a higher ionic conductivity of VCOF-SPE.

Besides the high ionic conductivity, the Li^+ transference number (t_{Li^+}) is another crucial factor for SPEs.^{47,48} Fig. 2c and S13† show the DC polarization curve and the AC impedance spectra for the Li|VCOF-SPE|Li symmetric cell setup at 60 °C, respectively. The value of t_{Li^+} was calculated to be 0.38, which is 46% higher than that of the Ref-SPE without VCOF-1 ($t_{\text{Li}^+} = 0.26$). The enhancement of the Li^+ transference number with the addition of VCOF-1 could be attributed to the immobilization of TFSI anions by VCOF-1, as it possesses a much stronger binding energy with the TFSI anion ($-428.6 \text{ kJ mol}^{-1}$) than what is observed for PEO with the TFSI anion ($-238.9 \text{ kJ mol}^{-1}$) (Fig. S12†). Moreover, the mechanical properties of the SPE were evaluated by tensile tests. The stress–strain curves in Fig. 2g show that VCOF-SPE possesses a tensile strength of 1.43 MPa, which is 11.9 times that of Ref-SPE (0.12 MPa). The superior mechanical properties of VCOF-SPE should also enhance the stability of the finally assembled batteries.

In summary, experimentally, PXRD identified PEO amorphization in VCOF-SPE, which is crucial for improved Li^+ conduction. FTIR, XPS, and ⁷Li ss-NMR revealed the distinct chemical environment of Li^+ within VCOF-SPE, while ⁷Li ss-NMR also showcased VCOF-SPE's superior Li^+ mobility compared to Ref-SPE. Additionally, DFT showed that axial Li^+ transportation, *i.e.*, along the VCOF-1 cylindrical pores, is markedly more efficient than planar Li^+ conduction. This efficiency is attributed to the shorter interlayer distance, which is enhanced by adjacent N atoms and assisted by PEO.

2.3 *In situ* observation of the Li dendrites

Fig. S14† shows the cross-section views of the tomography cell and corresponding average thickness at different temperatures.

The average thickness increased merely by 1.6% (from 618 to 628 μm) when the cell temperature increased from ambient to 70 °C, indicating the good dimensional stability of VCOF-SPE at an elevated temperature. The growth of Li dendrites at the interface of the SPEs was directly observed by *in situ* X-ray tomography. The measurements were conducted by applying symmetric Li|SPE|Li tomography cells (ESI Section 3.2†) at a working temperature of 60 °C. The cell was charged and discharged at 0.1 mA cm^{-2} for 1 hour repetitively to allow the Li stripping plating processes. Fig. 3a and b show the time-dependent voltage profiles of the cells with VCOF-SPE and Ref-SPE over 300 hours, respectively. The VCOF-SPE cell exhibited impressively high stability throughout the cycling process (Fig. 3a). In contrast, the cycling profile of the Ref-SPE-based cell in Fig. 3b shows a steady voltage increase *versus* the running time. This increasing stripping/plating voltage is similar to the liquid electrolyte behavior, typically resulting from the unstable Li deposition and continuous solid electrolyte interphase (SEI) formation at the electrode/electrolyte interface.⁴⁹ The large polarization of the Ref-SPE-based cell indicated its much higher internal resistance and lower ionic mobility as well. Short-circuit occurred in the Ref-SPE-based cell after 300 hours, indicating the Li dendrite penetration through the Ref-SPE due to its poor mechanical strength.

In situ X-ray tomography (see details in ESI Section 3.2†) illustrated the morphological evolution of the Li foil at the original state and after 150, 200, and 300 hours of Li plating/stripping using the VCOF-SPE and Ref-SPE (Fig. 3c and d). Remarkably, the addition of VCOF-1 substantially suppressed dendrite formation throughout the 300 hour stripping/plating process (Fig. 3c). In contrast, the Ref-SPE showed evident growth of Li dendrites on the electrode after 200 hours (Fig. 3d). This observation is consistent with the voltage profile of the Ref-SPE-based cell in Fig. 3b, in which a short circuit occurred after 310 hours due to the problematic Li dendrite growth and penetration through the SPE. Thus, the advantage of VCOF-SPE over the Ref-SPE toward Li dendrite suppression is revealed, which could be attributed to the synergistic effects of enhanced mechanical strength and improved Li-ion conductivity and Li-ion transference number. The enhanced mechanical strength (Fig. 2g) could restrain the growth of Li dendrites, and the significantly improved Li-ion conductivity and Li-ion transference number inhibit the formation of a Li^+ gradient at the electrolyte–electrode interface. Fig. S15† demonstrates the galvanostatic cycling for SPEs at various current densities to determine the critical current density (CCD) for VCOF-SPE and Ref-SPE. As expected, the voltage of the cells increased with increasing current densities. The critical current density of VCOF-SPE is 0.55 mA cm^{-2} , which is higher than that of Ref-SPE (0.30 mA cm^{-2}) at 60 °C, indicating a stable interface between the lithium metal anode and VCOF-SPE membrane. Fig. S16† shows the rate performance of Li|VCOF-SPE|Li and Li|Ref-SPE|Li cells at different current densities of 0.05, 0.1, and 0.2 mA cm^{-2} . The voltage increased as expected with increasing current densities for the VCOF-SPE and Ref-SPE membranes. The Li|VCOF-SPE|Li cell shows stable cycling with low voltage hysteresis throughout a 900 min cycle, indicating the favourable





Fig. 3 Inhibition of Li dendrites by VCOF-SPE. Stripping/plating profiles of (a) VCOF-SPE and (b) Ref-SPE samples over 300 hours at 60 °C. Tomography images of lithium electrodes inside a tomography-cell using (c) VCOF-SPE and (d) Ref-SPE after 0, 150, 200, and 300 hours of stripping/plating at a current density of 0.1 mA cm⁻² and working temperature of 60 °C.

Li plating/stripping kinetics and superior interface properties. In comparison, the Li|Ref-SPE|Li cell exhibits stable cycling with high voltage hysteresis.

2.4 Half-cell performance of VCOF-SPE in a Li|VCOF-SPE|LFP coin cell

The performances of VCOF-SPE were further investigated in a coin cell made of LiFePO₄ (LFP) as the cathode, VCOF-SPE as the electrolyte, and Li metal as the anode. The working temperature was maintained at 60 °C during electrochemical testing. Fig. S17[†] shows the CV curves of the cell at different cycles. A cathodic peak and an anodic peak were observed. The CV curves overlap after three cycles, suggesting its excellent electrochemical reversibility. Fig. S18[†] shows the linear sweep voltammetry (LSV) curves of VCOF-SPE and Ref-SPE. LSV was recorded by using an electrochemical workstation between 0 V and 6 V at a scanning rate of 0.1 mV s⁻¹. As seen, VCOF-SPE is stable in the voltage range from 2.5 to 4.0 V and starts to decompose at around 4.6 V. Fig. 4a illustrates the discharge/charge profiles of the VCOF-SPE-based coin cell at 0.1C. The cell was tested to achieve a high capacity of ~145 mA h g⁻¹. The first cycle showed a discharging capacity of 142.6 mA h g⁻¹, which then decreased slightly in the subsequent 100 cycles while maintaining an excellent coulombic efficiency of ~100% (Fig. 4b). In comparison, the battery based on Ref-SPE exhibited much lower capacities of 109.2 mA h g⁻¹ at 0.1C, which further decreased to 62.2 mA h g⁻¹ after 68 cycles (Fig. S19[†]). Fig. 4c reveals the battery capacities at various current densities for the VCOF-SPE-based battery, in which 136.3, 127.4, 120.4, 115.2,

and 111.2 mA h g⁻¹ discharge capacities were recorded at 0.2, 0.4, 0.6, 0.8, and 1.0C, respectively. The Ref-SPE based battery exhibited much lower discharge capacity compared to that with VCOF-SPE at different current densities. The results prove the excellent rate ability of VCOF-SPE to adapt to various current densities. To investigate the stability of VCOF-SPE against repeated Li⁺ intercalation/de-intercalation, the cell was maintained at a high current density of 0.5C for 120 cycles (Fig. 4d). A positive output discharge capacity was maintained at an average of ~120 mA h g⁻¹ with 85% capacity retention. The discharge capacity of the LFP|VCOF-SPE|Li cell is much higher than that of LFP|Ref-SPE|Li at 0.5C due to the higher conductivity of VCOF-SPE. When cycling at 0.5C, the capacity of the Ref-SPE-based battery first increases before decreasing, which indicates a process of interfacial contact improvement. In comparison, the VCOF-SPE-based battery exhibited gradual and gentle capacity decay, indicating that the interfacial contact is stabilized within the first cycle. This can be attributed to the good compatibility of VCOF-SPE, which contributes to a stable interface between VCOF-SPE and electrodes. Besides, the LiNi_{0.8}Co_{0.1}Mn_{0.1}O₂(NCM₈₁₁)|VCOF-SPE|Li and LiNi_{0.5}Mn_{1.5}O₄(LNMO)|VCOF-SPE|Li cells were further assembled to investigate the scope of use of VCOF-SPE. However, these cells cannot work normally. It is reported that pure PEO starts to oxidize at a voltage above 3.9 V *versus* Li/Li⁺.⁵⁰ Besides, the electrochemical stability window of the polymer electrolyte, as determined by the LSV method, is overestimated.⁵¹ Since the charging voltage of the NCM₈₁₁ and LNMO based half-cell is higher than 4.0 V, a Ni-based cathode with strong oxidizing properties could result in the decomposition of PEO-based SPEs.





Fig. 4 Half-cell performance of VCOF-SPE in a Li|VCOF-SPE|LFP coin cell. (a) Charge/discharge profile, (b) cycling ability at 0.1C current density, (c) rate performance at different C-rates, and (d) cycling performance at a high current density of 0.5C (1C = 170 mA g⁻¹).



Fig. 5 Pouch-cell performance and the abuse test of VCOF-SPE. Electrochemical performance of the LFP cathode in a Li metal pouch-cell using the VCOF-SPE: (a) charge/discharge profiles and (b) specific capacity and coulombic efficiency at 0.1C current density. (c and f) The LFP|VCOF-SPE|Li pouch cell lights a LED bulb. Abuse tests of the LFP|VCOF-SPE|Li pouch cell after being (d) slightly folded, (e) completely folded, (g) pierced, and (h) cut.

2.5 Pouch-cell performance and the abuse test of VCOF-SPE

To further demonstrate the potential of VCOF-SPE for practical applications, LFP|VCOF-SPE|Li pouch cells were assembled and tested. The electrochemical performances of the pouch cells were tested at 0.1C (Fig. 5a and b). The delivered capacity reached 80 mA h g⁻¹ at the initial cycle and stabilized at 131.5 mA h g⁻¹ after 20 cycles. The capacity increase is associated with an electrochemical activation process of the cell, mainly attributed to the gradual improvement of interfacial contacts between the electrodes and the SPE, caused by the lack of stacking pressure in pouch cells. After activation, the cell showed excellent cycling stability, with ~100% retention over 100 cycles (Fig. 5b). The assembled LFP|VCOF-SPE|Li pouch cells also demonstrated high flexibility and safety, which was revealed by abuse tests. As shown in Fig. 5c, the pouch cell was connected to a red light-emitting diode (LED). After slightly and completely folding the pouch cell, the LED remained lit (Fig. 5d and e). Moreover, the cell could still function and light the LED after nail penetration (Fig. 5g) and even cut by more than half (Fig. 5h), demonstrating its high safety.

3 Conclusions

In summary, we developed a chemically stable vinylene-linked COF functionalized SPE (VCOF-SPE) that is composed of VCOF-1/PEO/LiTFSI/PVDF. The addition of VCOF-1 enabled favorable migration of Li⁺ along the cylindrical channels in VCOF-1, facilitating Li⁺ conduction in SPE. The growth of Li dendrites at the Li/VCOF-SPE interface was remarkably inhibited, benefiting from the synergistic effects of improved Li-ion



